JOURNAL OF RHEOLOGY®

Unsteady flow and particle migration in dense, non-Brownian suspensions

Michiel Hermes, Ben M. Guy, Wilson C. K. Poon, Guilhem Poy, Michael E. Cates, and Matthieu Wyart

Citation: Journal of Rheology **60**, 905 (2016); doi: 10.1122/1.4953814
View online: http://dx.doi.org/10.1122/1.4953814
View Table of Contents: http://scitation.aip.org/content/sor/journal/jor2/60/5?ver=pdfcov
Published by the The Society of Rheology

Unsteady flow and particle migration in dense, non-Brownian suspensions

Michiel Hermes,[a] Ben M. Guy, and Wilson C. K. Poon

School of Physics and Astronomy, The University of Edinburgh, King's Buildings, Peter Guthrie Tait Road, Edinburgh EH9 3FD, United Kingdom

Guilhem Poy

Laboratoire de Physique, École Normale Supérieure de Lyon, Université de Lyon, 46 Allée d'Italie, 69364 Lyon Cedex 07, France

Michael E. Cates

DAMTP, Centre for Mathematical Sciences, University of Cambridge, Wilberforce Road, Cambridge CB3 0WA, United Kingdom

Matthieu Wyart

EPFL SB ITP PCSL, BSP 29 (Cubotron UNIL), Rte de la Sorge, CH-1015 Lausanne, Switzerland

(Received 12 November 2015; final revision received 4 May 2016; published 12 September 2016; corrected 20 September 2016)

Abstract

We present experimental results on dense corn-starch suspensions as examples of non-Brownian, nearly hard particles that undergo continuous and discontinuous shear thickening (DST) at intermediate and high densities, respectively. Our results offer strong support for recent theories involving a stress-dependent effective contact friction among particles. We show, however, that in the DST regime, where theory might lead one to expect steady-state shear bands oriented layerwise along the vorticity axis, the real flow is unsteady. To explain this, we argue that steady-state banding is generically ruled out by the requirement that, for hard non-Brownian particles, the solvent pressure and the normal-normal component of the particle stress must balance separately across the interface between bands. (Otherwise, there is an unbalanced migration flux.) However, long-lived transient shear bands remain possible. © *2016 The Society of Rheology*.
[http://dx.doi.org/10.1122/1.4953814]

I. INTRODUCTION

Newtonian liquids, such as water, ethanol or honey, are each characterized by a well-defined, shear-rate-independent viscosity η. In contrast, many complex fluids, such as particulate suspensions, surfactant solutions, and polymer solutions, show shear thinning and/or shear thickening, so that their steady-state viscosity depends on the shear rate $\dot{\gamma}$. The shear stress plotted as a function of shear rate $\sigma(\dot{\gamma}) = \eta(\dot{\gamma})\dot{\gamma}$, known as the flow curve, then has a slope less than or greater than unity, for shear thinning or shear thickening, respectively, when plotted on logarithmic axes.

In extreme shear thinning or thickening systems, there can in principle appear regions of the flow curve where $\partial\sigma(\dot{\gamma})/\partial\dot{\gamma} < 0$ for a range of flow rates. Homogeneous flow is then mechanically unstable [1]. In many such cases, there exist inhomogeneous, shear-banded states that allow the system to flow steadily in time despite this instability. These involve either bands oriented layerwise along the vorticity direction with the same shear rate but different shear stresses (vorticity banding), or bands oriented in the gradient direction with the same shear stress but different shear rates (gradient banding). There are cases, however, where such banded flows are themselves unstable, giving rise to time-dependent flows with fluctuating shear stresses and rates. These unsteady flows vary from relatively simple oscillations to fully developed chaos; shear-band-like features may or may not remain detectable.

These chaotic flows arise from viscoelastic instabilities at essentially zero Reynolds number (negligible inertia), in contrast to conventional fluid turbulence; they are sometimes called "rheochaos." Viscoelastic instabilities are relatively well studied in entangled micellar systems. In that context, they are often interpreted in terms of an interplay between a slow fluid relaxation time (Maxwell time, τ_M) and an even slower process that modulates τ_M [2]. However, rheochaos can equally arise in systems without this timescale separation, such as simple nematic fluids [3].

In this paper, we present detailed experimental evidence for unsteady flow (leading to rheochaos) in a shear-thickening suspension and explore the various regimes that

[a]Author to whom correspondence should be addressed; electronic mail: michielhermes@colloids.nl

emerge. The suspension is granular, rather than colloidal, comprising particles that are large enough for Brownian motion to be negligible. Its flow curve is predicted theoretically to be nonmonotonic, in a way that might normally be expected to support steady shear bands. Without Brownian motion, however, we will argue that such bands are generically disallowed, so that the flow is unsteady.

Perfectly hard spheres have functioned as a conceptual model for the rheology of particulate suspensions for a long time [4,5] and continue to yield many insights, e.g., in the study of viscosity divergence near glassy arrest [6]. As two idealized hard spheres approach each other through a fluid with no-slip boundary conditions, the time taken to drain the layer of fluid between them (the lubrication film) diverges, and large "lubrication forces" prevent the particles from ever making contact. However, if the particles are slightly rough, or have a finite slip length, they can come into contact when the lubrication film reaches a thickness comparable to the surface roughness or the slip length. In practice therefore, direct contact forces certainly play a role in real "hard-sphere" suspensions [7], and these contact forces can be expected, in general, to include static friction.

Surprisingly, at low volume fraction, ϕ, the viscosity of a suspension of spheres in frictional contact is *lower* than that of an identical suspension of smooth spheres [8]. The opposite holds at high ϕ, where frictional contacts have recently been demonstrated by experiments [9,10], simulations [11–14], and theory [15] to play a crucial role in shear thickening, and ultimately jamming.

These recent advances formalize and develop earlier insights from Melrose and Ball (MB). In their simulations of non-Brownian spheres [16], MB found that the gap between the surface of particles, d, could fall to molecular dimensions in a real suspension, giving rise to numerically diverging lubrication forces (which scale as d^{-1}). MB overcame this problem by introducing a short-range repulsive force that stops these pathologically small gaps from forming [17]. In a real suspension, such repulsion can arise from stabilizing polymers and/or charges on particle surfaces. Significantly, MB pointed out that the "small gap problem" would recur above a stress $\sigma^\star$ at which the stresses in the system overcome these stabilizing repulsions. Crucial to recent advances is the realization that, when the force threshold for a particular contact is exceeded, its lubrication film may fail immediately (due to roughness or a finite slip length) allowing the particles to come into direct frictional contact. Thus the "onset stress" $\sigma^\star$ marks a crossover from open, well lubricated (or sliding) contacts between particles to direct, frictional (or rolling) contacts.

Developing this insight, Wyart and Cates [15] (WC) have constructed a phenomenological theory for the steady flow of shear-thickening particulate suspensions. They take all particle interactions to be lubricated (frictionless) when $\sigma \ll \sigma^\star$ so that the system is quasi-Newtonian with a viscosity that diverges at random close packing $\phi_0 = 0.64$. However, when $\sigma \gg \sigma^\star$, all contacts are frictional and the system is again quasi-Newtonian, but now with a viscosity diverging at some lower volume fraction, $\phi_m < \phi_0$, whose value depends on the interparticle static friction coefficient, μ_p [12]. The transition between these two regimes on increasing σ causes shear thickening.

This scenario resolves a longstanding puzzle in dense suspension theory. Strictly hard particles can have no stress scale $\sigma^\star$, and, without Brownian motion, also have no timescale at rest. Hence, all stresses must scale linearly with $\dot\gamma$ [18]. (This includes nonvanishing normal stresses, which is why we describe the two limiting branches as quasi-Newtonian, not Newtonian.) Thus, in the absence of Brownian motion and inertia, shear-thickening requires some deviation from strict hard sphere behavior. The key idea of recent work is that this deviation provides, in effect, a stress-dependent interparticle friction [11,15,19].

In this paper, we study the rheology of corn-starch suspensions below and above ϕ_m. Above ϕ_m, complete jamming is expected, surprisingly, however, we show that flow is still observed, but is always unsteady, and shows rheochaos at high enough stress. This relates to the fact that you can run, but not stand still, on a pool of corn starch. Similar unsteadiness is seen for $\phi_c < \phi < \phi_m$, so that the entire discontinuous shear thickening (DST) region is affected. After describing these results, we give arguments that unsteady flow should, on theoretical grounds, be a generic feature of dense particulate suspensions in the DST regime.

II. METHODS AND SETUP

Rheological measurements were performed with a stress-controlled rheometer (DHR-2, TA Instruments) with hatched parallel plates, $R = 40$ mm diameter [Figs. 1(a) and 2] or with a Couette cell (inner diameter of 18 mm, outer diameter 21 mm) and roughened boundaries [Fig. 1(b)] at a temperature of 20 °C. We obtained the raw torque and strain data at a rate of $\sim 10^3$ Hz using the TA software tool "ARG2AuxiliarySample." The sample was imaged from the side using a digital camera at a frame rate of 30 fps using a 16 mm macro-objective.

We performed experiments on corn starch (Sigma Aldrich, unmodified regular corn starch containing approx. 73% amylopectin and 27% amylose [S4126]; diameter $\approx 14\,\mu$m, polydispersity $\approx 40\%$ from static light scattering) dispersed in a mixture of 50 wt. % water and 50 wt. % glycerol (viscosity $\eta_s = 6$ mPa s, density $\rho_s = 1.17$ g cm^{-3}) at various concentrations. The particles swell in our solvent, so that we cannot access the volume fraction 0. We therefore quote mass fractions ϕ^w. Samples were freshly mixed for each experiment and rested for several minutes before loading into the rheometer. Sedimentation and evaporation begin to influence the rheology after ~ 30 min with parallel plates; we discard data taken after this time.

Flow curves, Fig. 1, were obtained by increasing the torque, M, continuously with a logarithmic rate from 0.1 to 1000 Pa over 300 s. Most samples show edge fracture at stresses between 100 and 1000 Pa; we do not show any data points for which this has happened. In parallel plate work, we report the shear rate at the rim of the plates $\dot\gamma = R\dot\varphi/H$, where H is the gap height, and the apparent shear stress, $\sigma = 2M/(\pi R^3)$.

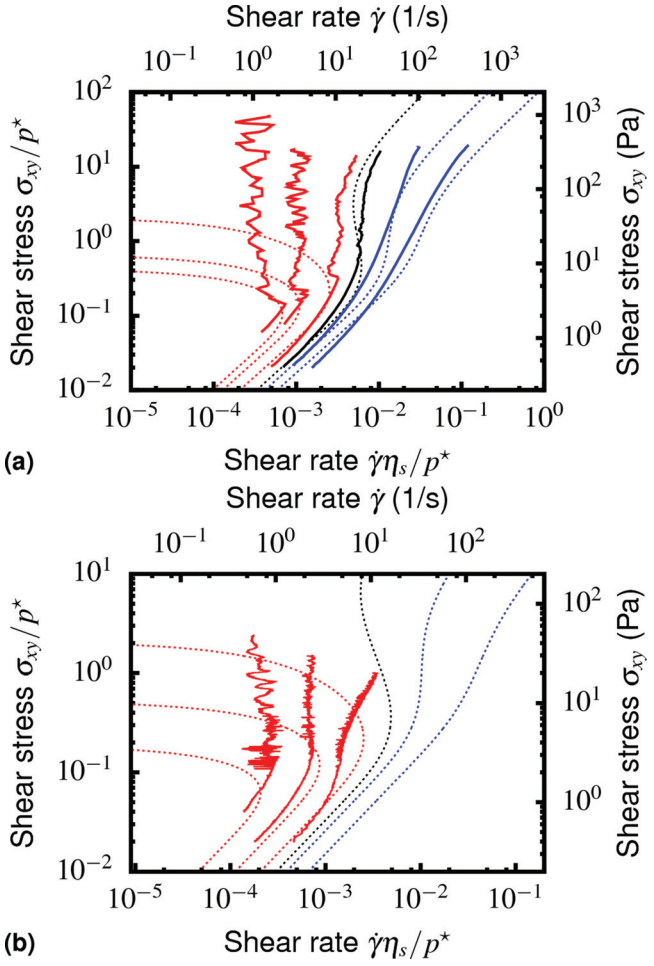

FIG. 1. (a) Apparent shear stress σ_{xy} vs rim shear rate $\dot\gamma$ for corn-starch suspensions at mass fractions $\phi^w = 0.45$, 0.46, 0.465, 0.47, 0.50, and 0.52 from right to left. Data represent upward stress sweeps measured between hatched plates. Stress is reported in Pa (right vertical axis) and in units of the onset pressure for shear thickening, $p^\star = 20.0$ Pa (left vertical axis). Shear rate is reported in s^{-1} (top horizontal axis) and reduced units $\dot\gamma\eta_s/p^\star$ (bottom horizontal axis). Dashed lines: prediction of Eq. (5) at different ϕ (0.50, 0.525, 0.54, 0.565, 0.585, and 0.595) with $\phi_m = 0.55$ and ($\phi_{RCP} = 0.66$; these volume fractions were chosen to match experimental data. (b) The same as above but measured using a Couette geometry, mass fractions $\phi^w = 0.47$, 0.50, and 0.53 from right to left. The dashed lines are predictions from theory for $\phi = 0.49$, 0.53, 0.545, 0.565, 0.595, and 0.615.

III. RESULTS

Figure 1 shows flow curves measured at different mass fractions, ϕ^w (see caption), reported as the reduced shear stress $\sigma/p^\star$, versus the reduced shear rate, $\dot\gamma\eta_s/p^\star$. Here, $p^\star$ is the onset pressure for the formation of frictional contacts, related to the onset stress through $\sigma^\star = \mu(\phi)p^\star$, see Sec. IV. (Note that we control the shear stress, plotted on the vertical axis, and measure the shear rate, on the horizontal axis.) At $\phi^w < \phi_c^w \approx 0.465$, we observe continuous shear thickening (CST) above an onset pressure $p^\star = 20.0 \pm 5$ Pa to a high-viscosity quasi-Newtonian state (blue curves in Fig. 1). The steepness of the shear-thickening part of the flow curve increases with ϕ^w until, at ϕ_x^w, $d\dot\gamma/d\sigma = 0$ beyond which the sample discontinuously shear thickens. In contrast to the continuous case, where the flow is steady throughout the flow curve, we now observe large shear-rate fluctuations above the critical stress, resulting in considerable spread in the data. These fluctuations are also present in constant stress experiments (as shown in Fig. 2) and remain present for long times (at least 30 min). Such large fluctuations arise as soon as the measured flow curve starts bending backwards. (Hence, there is no inconsistency in the apparent negative slopes of the empirical, averaged, "flow curves.")

Just above ϕ_c^w [black curve, Fig. 1(a), measured between hatched parallel plates], there is a narrow concentration range in which the system can reach a flowing quasi-Newtonian state at high stresses, as previously reported [20], although we observe severe deformations of the meniscus in this regime. Above a second critical concentration $\phi_m^w \approx 0.47$ [red curve, Figs. 1(a) and 1(b)], no such quasi-Newtonian regime is found even at the highest observable stresses; instead the flow is always erratic. We observe very similar behavior in a Couette geometry, Fig. 1(b). These time-averaged observations map rather directly onto the WC theory of steady-state shear thickening if we identify ϕ_c^w with ϕ_c, the point where sigmoidal flow curves emerge, and ϕ_m^w with ϕ_m, the jamming point for frictional particles. On the other hand, the theory does not capture the magnitude of the shear thickening completely, most likely due to the wide size and shape dispersity in corn-starch, or nonhard interactions, which also give rise to a small yield stress (not shown).

Significant differences between experiments and theoretical expectations (see Sec. IV) arise for $\phi > \phi_m$. Here, WC theory leads us to expect that no steady flow is possible above a threshold of stress, even with shear bands present, because there is no upper branch to the flow curve. However, at low stresses, steady flow is possible on the lower branch, but beyond it, the only steady state either has coexistence of low and high stress bands, both at $\dot\gamma = 0$, or is jammed homogeneously (again with $\dot\gamma = 0$). Thus, one might expect the system to be able to support a relatively modest static load without flowing at all.

However, these WC scenarios refer to steady states. Experimentally, we find instead that the system *does* flow at high stresses in this regime, but flows unsteadily. The phenomenology of this "unexpected" flow at $\phi > \phi_m$ is complex. To begin to explore it, Fig. 2(f) shows the time-averaged flow curve, as well as the measured fluctuations, in a sample at $\phi^w = 0.50$, corresponding to a volume fraction just above ϕ_m. At the lowest applied shear stresses, $\sigma < 0.1p^\star$, the shear rate fluctuates only a little around a well-defined average [see Fig. 2(a)]. The axial stress measured on the top plate, N, is close to the noise level of the transducer [21]. The meniscus at the air-sample interface remains smooth, shiny, and undisturbed. We observe a drift in the shear rate after long times (hours), presumably due to particle migration, sedimentation, or evaporation.

For $0.1\sigma^\star \lesssim \sigma \lesssim 0.2p^\star$, region B in Fig. 2(f), the flow is steady for seconds, but is punctuated by sudden drops in $\dot\gamma(t)$, Fig. 2(b). We refer to these events as "jams," and argue that they are related to the formation of locally solid regions within the suspension. During a jamming event, $\dot\gamma$ (purple and red lines) drops rapidly, with a concomitant positive spike in the axial stress (black lines), before increasing slowly back to the steady-state value.

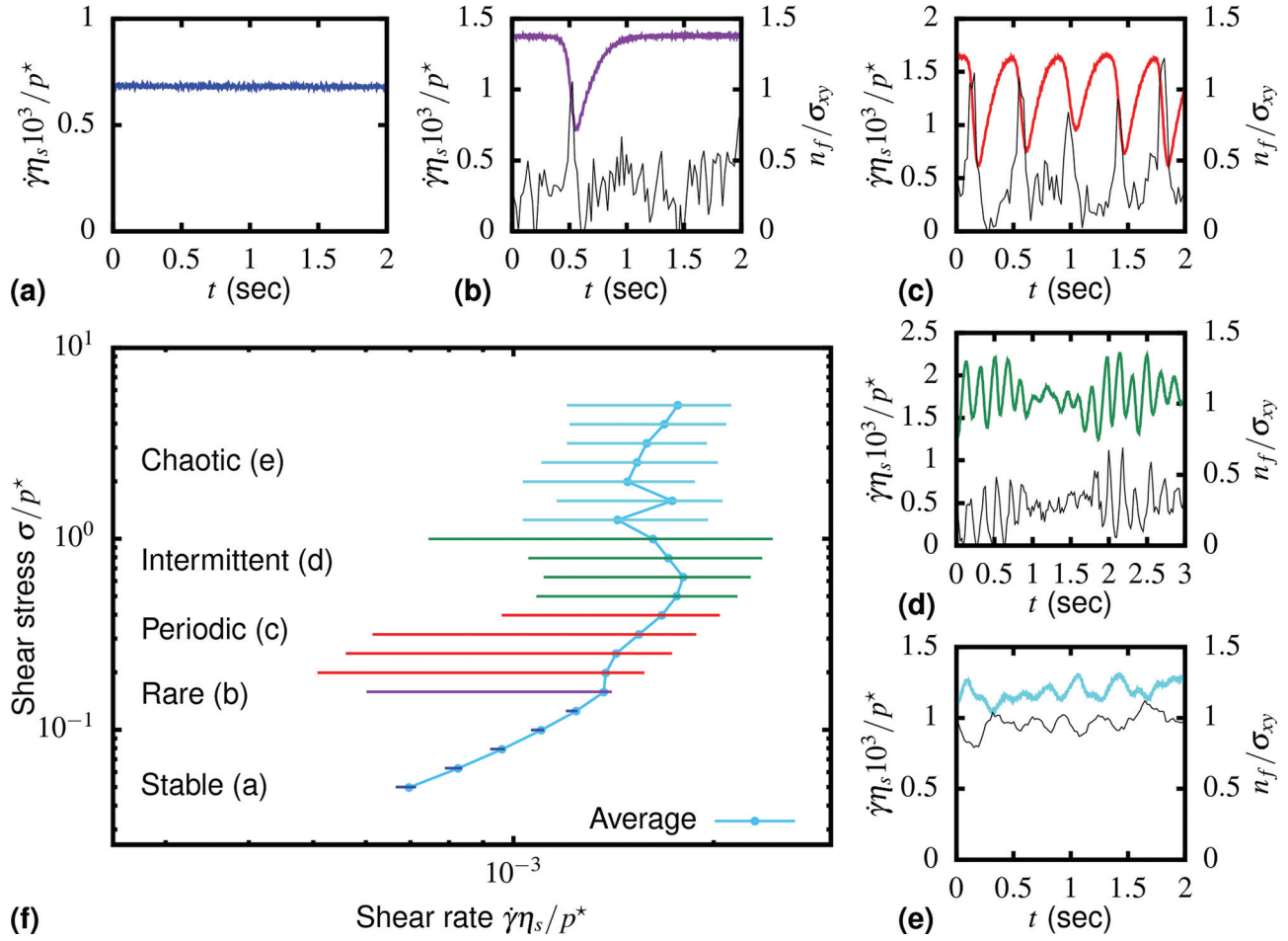

FIG. 2. (a)–(e) Apparent shear rate as a function of time for increasing stress, on the left y axis. The thin black lines show the normal pressure n_f/σ_{xy} on the right y axis. (f) Apparent shear stress as a function of rim shear rate $\dot{\gamma}_R$ in absolute and reduced units for corn starch at a mass fraction of $\phi^w = 0.52$, corresponding to a volume fraction just above ϕ_m in WC theory. Horizontal lines: raw $\dot{\gamma}_R$ data at different applied σ_{xy} in the stable (dark blue), periodic (red), intermittent (green), and chaotic (cyan) regimes. Symbols: average $\dot{\gamma}_R$.

While the jamming events in region B are sparsely distributed and seem to occur randomly in time, they become very regular with a well-defined frequency at $\sigma \gtrsim 0.2p^\star$, regime C Fig. 2(f). This is visible macroscopically as periodic jerks of the rheometer top plate. The minimum shear rate reached during a jamming event is variable, Fig. 2(c), while the shear rate in the flowing state is approximately the same and corresponds to the right-hand limit of the horizontal lines in Fig. 2(f). These oscillations remain over long times and only change over the course of hours (presumably as the sample dries out). The frequency of the oscillations increases linearly with the applied stress, Fig. 3(a). Each sudden decrease in $\dot{\gamma}$ is accompanied by a localized deformation of the air-sample interface. A small area of the interface comparable to the gap height bulges out slightly, while the surrounding area curves slightly inward. The interface recovers a smooth profile as the plate accelerates back to the steady-state value. Note that these localized jams are not an artifact of the cross-hatched plates; they start to appear at the same stresses with smoother surfaces, albeit in the presence of significant wall slip, as well as in Couette geometries [Fig. 4(b)].

In region D, Fig. 2(f), periodic jamming coexists temporally with bursts of unpredictable fluctuations, as shown in Fig. 2(e). During the periodic intervals, the air-sample interface behaves the same as in region C, with short-lived, static jammed regions appearing at the same time as the drop in shear rate. During the random bursts, more irregular surface deformations are observed that are long lived and move around the interface opposite to the direction of flow [see Figs. 3(b)–3(d)]. Usually, only one or two transient deformations appear during each intermittent event and disappear when the periodic oscillations resume.

At the highest stresses $\sigma/p^\star \gtrsim 1$, in region E, Fig. 2(f), the periodic jamming and unjamming are absent, and only random-looking fluctuations are observed, Fig. 2(e). This behavior, and the series of events at lower stresses that precede it, are similar to the development of rheochaos as observed in micellar systems [2]. We leave it to future work to establish whether the flow is really chaotic in a technical sense; for our purposes, what matters is that it is unsteady, not readily predictable, and without obvious periodic features. In region E, the first normal stress difference is permanently large and positive and anticorrelated with the shear rate. Very recently, unstable flow, sudden jams and a transition to what appears to be rheochaos have been observed in 2D computer simulations of inertial frictional grains [22]. Although the origin of the sigmoidal flow curves is different,

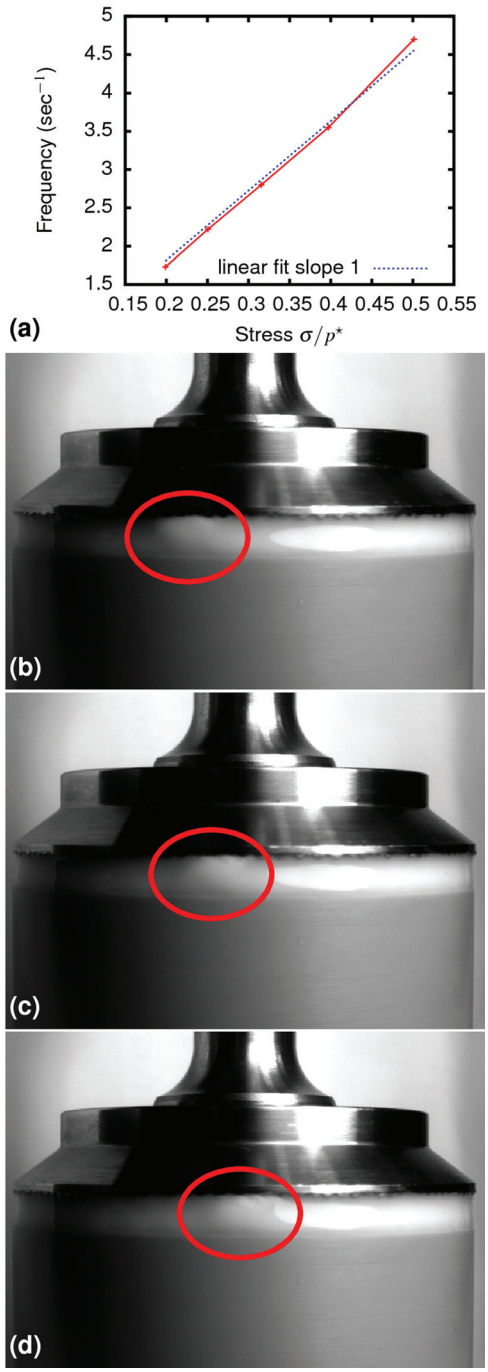

FIG. 3. (a) The frequency of the oscillation as a function of the applied stress for a sample at $\phi^w = 0.50$ measured between hatched plates. (b)–(d) Pictures of the deformation of the interface during the intermittent regime d at $\phi^w = 0.50$ between hatched plates. In the photos, the front of the cone rotates to the left, the gray bottom plate is stationary, and a deformation of the interface (highlighted by a red ellipse) moves to the right.

the types of unstable flow observed there are very similar to the ones reported here.

We observe the same transition sequence in a Couette geometry as with parallel plates, although the onset stress for unsteady flow is lower in a Couette geometry than between parallel plates, Figs. 4(a)–4(e). We observe the same sequence of phenomena for other volume fractions above ϕ_m, whereas for samples just below ϕ_m, we observe an additional steady flow regime at high stress, Fig. 4(j). At lower volume fractions, we do not observe shear rate fluctuations at any applied stress, Figs. 4(k)–4(o).

IV. THEORY

In this section, we will summarize the steady-flow theory outlined in [15]. We will then explore what this means for the stability of the flow of shear thickening suspensions. WC describe the rheology of dense non-Brownian suspensions with a jamming volume fraction, $\phi_J(p)$, that depends on p, the particle pressure, defined via the trace of the particle contribution to the stress. This $\phi_J(p)$ evolves smoothly from $\phi_J(p) = \phi_0$ to $\phi_J(\infty) = \phi_m$ as the fraction of frictional contacts f goes from 0 to 1

$$\phi_J(p) = \phi_m f(p/p^\star) + \phi_0[1 - f(p/p^\star)]. \tag{1}$$

Here, f, which is dimensionless, can depend only on the ratio of p to the onset stress, as written above. The precise form of f is inessential, but a stretched exponential

$$f = \exp\left[(-p^\star/p)^\beta\right] \tag{2}$$

gives good agreement with experiments [9] and simulations.

At the macroscopic level, the particle pressure ϕ is related to the shear stress σ through a stress ratio or macroscopic friction coefficient $\mu(\phi)$ (not to be confused with μ_p as defined above)

$$\sigma = \mu(\phi)p, \tag{3}$$

where μ is taken by WC to depend only on ϕ. This involves a simplification, since in principle the macroscopic friction coefficient μ could certainly also depend on the state of microscopic friction and hence on f [15,23,25]. We return to this issue below. This relation between stress and pressure allows us to write Eq. (1) as function of stress instead of pressure

$$\phi_J(\sigma) = \phi_m f(\sigma/\sigma^\star) + \phi_0[1 - f(\sigma/\sigma^\star)], \tag{4}$$

where $\sigma^\star = \mu(\phi)p^\star$.

Finally, the suspension viscosity $\eta = \sigma(\dot\gamma)\dot\gamma$ is known to diverge as the jamming transition is approached [23]. This divergence is related to the explosion of velocity fluctuations caused by excessive crowding [26,27] and can be computed in simple models [28]. In WC, this effect leads to a divergence of viscosity at $\phi_J(P)$ modeled as

$$\eta(\sigma,\phi) = \sigma/\dot\gamma = \eta_s\left[1 - \frac{\phi}{\phi_J(\sigma/\mu(\phi))}\right]^{-\alpha} \tag{5}$$

with an exponent estimated as $\alpha = 2$. This leads to S-shaped flow curves, whose likely role in shear thickening was earlier identified in [29].

Figure 5(a) shows the reduced suspension viscosity, $\eta(\sigma,\phi)/\eta_s$, predicted by the WC model as a function of

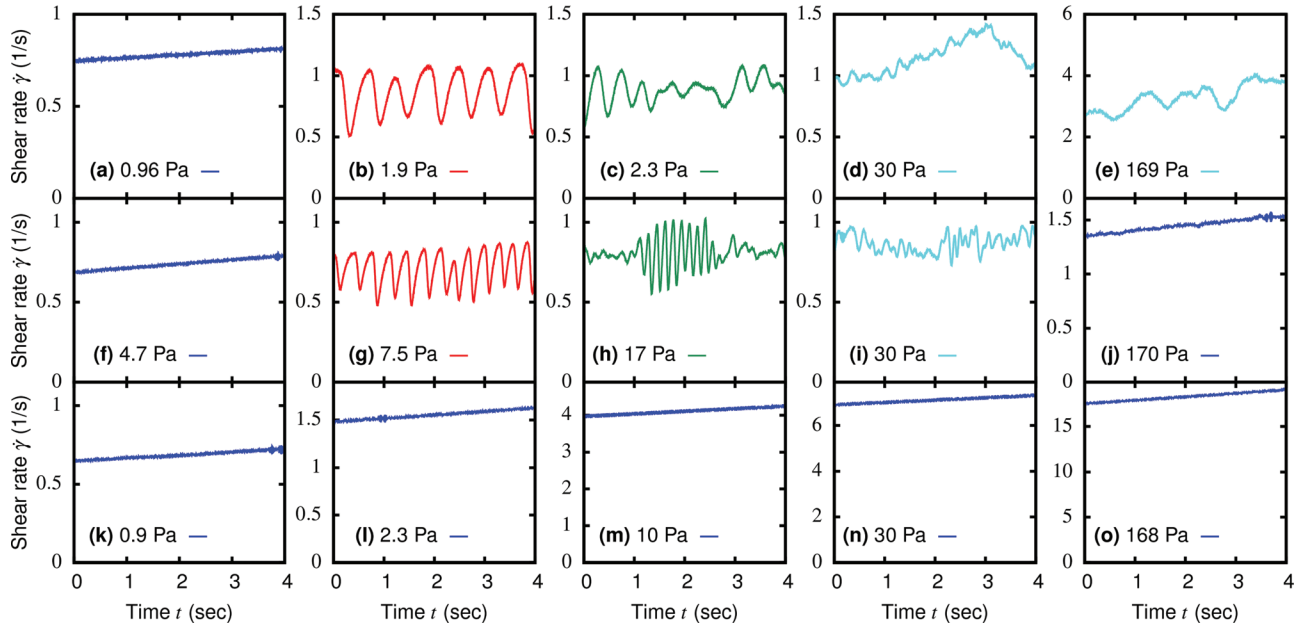

FIG. 4. (a)–(e) Apparent shear rate as a function of time measured during a continuous increase in shear stress in a Couette geometry at $\phi^w = 0.50$. (f)–(j) Same as (a)–(e) but in a parallel plate geometry at $\phi^w = 0.465$. (k)–(o) Same as (a)–(e) but in a parallel plate geometry at $\phi^w = 0.45$.

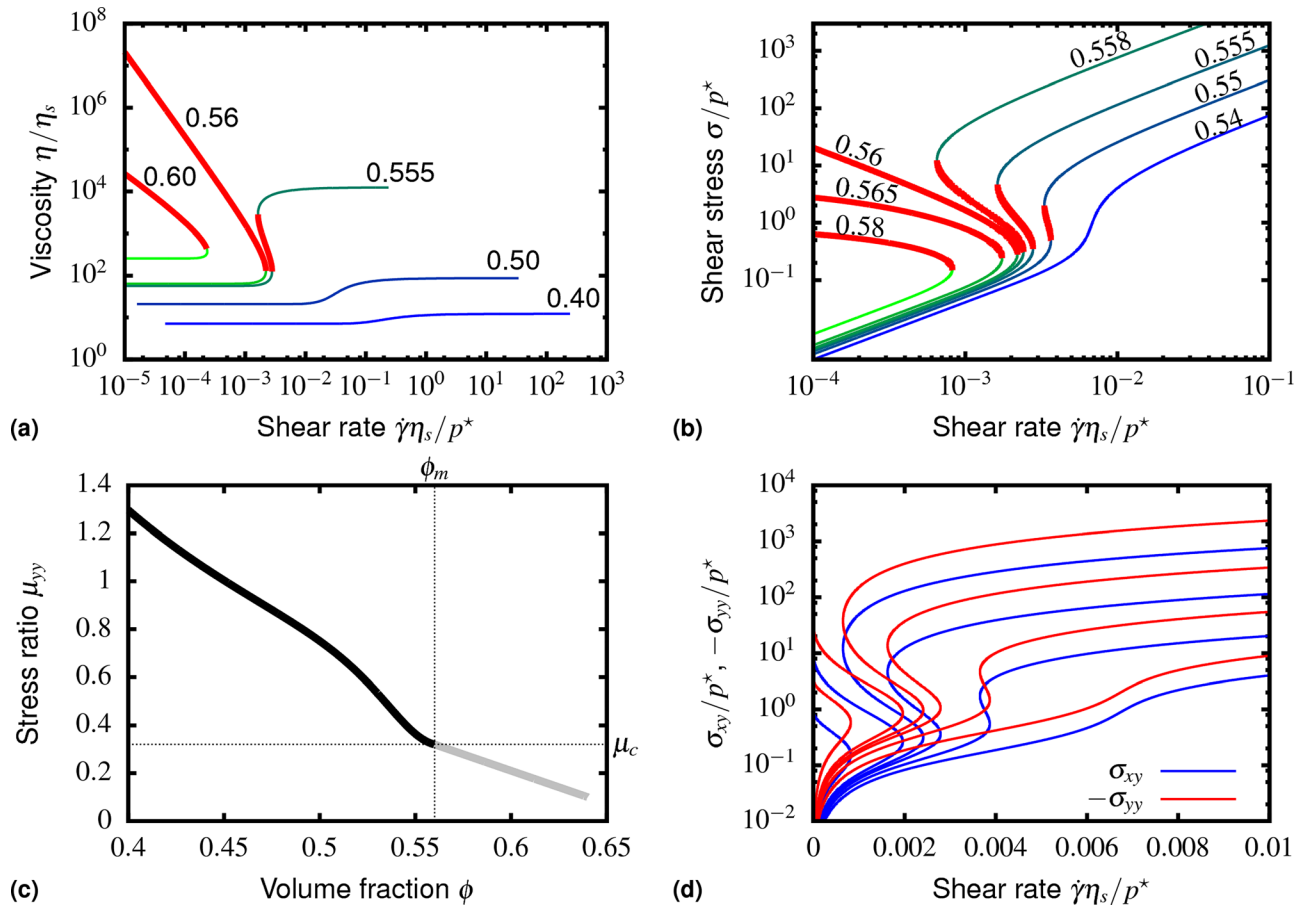

FIG. 5. (a) Relative viscosity η/η_s vs reduced shear rate $\dot{\gamma}\eta_s/p^\star$ at different volume fractions ϕ (as labeled) predicted by the theory of Wyart and Cates [15], [Eq. (5)]. We take $\phi_m = 0.56$, $\phi_{\mathrm{RCP}} = 0.64$, $\beta = 1$ from recent experiments [9]. The unstable regimes are marked in thick (red) lines. (b) Corresponding flow curves (shear stress as a function of shear rate). (c) The ϕ-*independent* stress ratio (or effective macroscopic friction coefficient) in the y- (gradient-) direction, $\mu_{yy} = \sigma_{xy}/\sigma_{yy}$, used to obtain these plots. Black solid line: derived from Boyer *et al.* [23], applicable up to ϕ_m; gray line: a plausible extrapolation to higher ϕ based on 2D simulations [24]. (d) The flow curves $\delta_{xy}(\dot{\gamma})/p^\star$ at different ϕ (blue lines) plotted again, now against a linear horizontal axis, and compared with the normal stress in the y-direction $-\sigma_{yy}(\dot{\gamma})/p^\star$ (red lines) calculated using the expression for μ, shown in (c).

reduced shear rate $\dot{\gamma}\eta_s/\sigma^\star$ using $\phi_0 = 0.64, \phi_m = 0.56$ and $\beta = 1$. For ϕ somewhat less than ϕ_m, the system shear thickens continuously between the two quasi-Newtonian regimes. The slope $d\eta/d\dot{\gamma}$ increases with ϕ until, at a critical $\phi = \phi_c \approx 0.55$, $\eta(\dot{\gamma})$ becomes vertical. For $\phi > \phi_c$, $\eta(\dot{\gamma})$ contains a region of negative slope and develops a sigmoidal shape, while tending toward quasi-Newtonian regimes at both low and high stresses. Above a second critical volume fraction set by $\phi = \phi_m$, the backward-bending part of the flow curve meets the vertical axis and there is no longer a flowing branch at high stresses. The corresponding $\sigma(\dot{\gamma})$ curves are shown in Fig. 5(b).

As ϕ is increased, the theory predicts first CST, then DST between two flowing branches each of finite viscosity [20], and finally DST from a flowing branch to a jammed branch that cannot flow at finite y without some sort of fracture [30]. This last regime, which arises for $\phi > \phi_m$, is called "complete jamming" [31]; in it, the putative upper branch of the flow curve $\sigma(\dot{\gamma})$ runs straight up the vertical axis. The WC model fits recent $\eta(\sigma, \phi)$ data on suspensions of sterically stabilized polymethyl methacrylate (PMMA) particles whose interactions closely approach the hard-sphere limit [9]. The predicted sigmoidal flow curves, although preempted by instability in bulk steady flows, have since been observed, at least transiently, in experiments and simulations of nearly hard non-Brownian particles [13,32].

At high volume fractions, in the complete jamming regime, the WC theory requires that any high-stress shear band must have zero flow rate, $\dot{\gamma} = 0$. This is because the only other frictional states on the flow curve have $d\sigma/d\dot{\gamma} < 0$ and are themselves unstable. Thus, any steady banded state comprises coexistence, layerwise along the vorticity direction, of a jammed state at finite stress and a fluid state at zero stress (since with this orientation, y is equal in both bands). Thus, no steady flow is possible even with shear bands present; the only steady flow states for $\phi > \phi_m$ are homogeneous and lie on the low-friction branch. Dynamically, if the mean shear stress is increased beyond the stability limit of that branch, one might then expect its local value to become increasingly heterogeneous along the vorticity direction until flow stops altogether for the reasons just described.

V. ABSENCE OF STEADY SHEAR BANDS

It is notable that in our experiments, we observe unsteady flow at all concentrations $\phi > \phi_c$ where stable banded flow may, at least at first sight, be expected. We now turn to explore the origins of these instabilities in our system.

Flow instability, oscillation, and rheological chaos have been fairly widely reported in both shear-thinning and shear-thickening viscoelastic materials (particularly but not exclusively micellar solutions [2]). Given the presence of highly nonlinear constitutive equations that relate stress to strain-rate history, one might expect instability to be more common. Mathematically, unsteady solutions can either arise "directly" from the instability of a steady homogeneous flow, or through a similar instability within one of the shear bands that would otherwise allow steady but inhomogeneous flow [33].

Although in general one does not expect simple rules to govern whether flows are steady or unsteady, dense non-Brownian shear-thickening suspensions present a somewhat special case in relation both to vorticity bands and to gradient bands. Below, we deal with these two cases in turn. We consider the case where the flow curve has a sigmoidal shape, which occurs for $\phi_c \le \phi < \phi_m$, as well as the regime $\phi > \phi_m$ (with no upper flow branch), which applies in most of the experiments presented above. We refer to the flow, gradient, and vorticity directions as x, y, and z, respectively.

Let us consider the diagonal components of the stress tensor, which comprise an isotropic solvent pressure $-p_s\delta_{ij}$ plus the three normal stresses $\sigma_{uu} = -p_{uu}$ caused by the presence of particles. (Here $u = x, y, z$ is a generic, but not summed, Cartesian index; recall the stress and pressure tensors have opposite signs.) For strictly hard spheres with fixed frictional properties, each normal stress is linear in $\dot{\gamma}$. More generally, we are dealing with a manifold of steady states in which the ratio of shear to normal stresses (i.e., the macroscopic friction constant) depends on both volume fraction and the state of contact friction captured by $f^{(\sigma)}$

$$-\sigma_{uu} = p_{uu} = \sigma_{xy}/\mu_{uu}(\phi, f(\sigma)). \tag{6}$$

Generically, the μ_{uu} are unequal, causing normal stress differences $N_1 = \sigma_{xx} - \sigma_{yy}$, and $N_2 = \sigma_{xx} - \sigma_{yy}$.

A simplification made by WC was to suppress the dependence of μ_{uu} on the state of contact friction, so that it is a function of ϕ only. This is pursued in Figs. 5(c) and 5(d), where $\mu_{uu}(\phi)$ is estimated as described in Appendix A, which also gives further information about what is known of the μ_{uu} s in granular systems. More generally, however, the μ_{uu} must depend on σ via $f(\sigma)$ as well as on ϕ; hence, the macroscopic friction will have different values on the lower and upper limiting branches of the flow curve. Therefore, each of the normal stresses has a shear rate dependence $p_{uu}(\dot{\gamma})$ that *qualitatively* resembles the shear stress $\sigma_{xy}(\dot{\gamma})$, but is not *quantitatively* proportional to it as was assumed in Fig. 5(d). This will prove important in the discussion of gradient bands below. First, however, we address vorticity bands.

A. Vorticity bands

We consider flow between infinite parallel plates so that homogeneous flow is possible in principle. Steady vorticity bands are expected to arise when the applied steady shear stress σ^a_{xy} falls within a window $\sigma^{(1)}_{xy} < \sigma^a_{xy} < \sigma^{(2)}_{xy}$ that includes all part of the flow curve with negative slope. (Vorticity bands are not expected to arise in experiments at controlled $\dot{\gamma}$ [1].) The vorticity bands have a common shear rate, $\dot{\gamma}_1 - \dot{\gamma}_2$, but different shear stresses $\sigma^{(1)}_{xy}$ and $\sigma^{(2)}_{xy}$ [see Fig. 6(a)]. As σ^a_{xy} is varied, the fraction of the sample occupied by each type of band adjusts so that the space-averaged shear stress is σ^a_{xy}.

Mechanical stability then requires equality between bands of the normal stress normal to the band interface, σ_{zz}. We

thus have $p_s^{(1)} + p_{zz}^{(1)} = p_s^{(2)} + p_{zz}^{(2)}$. The particle contribution p_{zz} is mediated by forces (perhaps including lubrication forces) which are in effect transferred directly from particle to particle through a network of contacts. The fluid pressure p_s is carried by solvent molecules that can move freely through the pores of this network. Without Brownian motion to create an osmotic reaction force, any difference in fluid pressure between bands should drive the solvent to flow from high to low p_s, with mass balance maintained by a flux of particles in the opposite direction, from high to low p_{zz}.

Thus, p_s and p_{zz} must be separately equal in shear-banded non-Brownian suspensions. Though the argument is general, it is particularly transparent for $\phi > \phi_m$, when coexisting vorticity bands are in fact at rest, as previously explained. No lubrication (or other hydrodynamic) forces then remain, so the fluid and particle mechanics are completely decoupled. It is quite clear in this case that the solvent and particle pressures *must* be separately equal between bands. The same argument extends to flowing bands, at least if the system is treated as two continua (solvent and particles) with a drag term coupling their two velocities (i.e., a two-fluid model) [34].

Steady vorticity bands thus require not only equal strain rate but also equal particle pressure p_{zz}. Since f is only a function of the particles pressure p_{zz} [Eq. (2)], the fraction of frictional contacts and thus the frictional states of the two bands must be identical (note that 0 itself can be seen as a function of f and p_{zz} [23]). However, if the frictional state has to be the same in both bands, then the suspension is identical to one with a fixed microscopic friction coefficient μ_p. Therefore, for vorticity bands to be stable, they also need to be stable for a system with a fixed friction coefficient. However, suspensions at fixed friction are well studied and shear banding has not been observed [23,25]. A supplementary argument, starting from the same premise and leading to the same conclusion that vorticity banding is prohibited in dense non-Brownian suspensions, is provided in Appendix B.

It is helpful to discuss separately the case when $\phi > \phi_m$ so that the bands are not flowing. The particle stresses in the fluid band vanish. In this case, equality of p_{zz} would require μ_{zz} to diverge on the frictional branch so that there is a large shear stress at vanishing normal stress. However, the frictional branch at $\phi > \phi_m$ is a jammed solid. Such materials can support only a finite stress anisotropy without flowing, so that p_{zz} cannot become infinite as required. Hence, coexistence of nonflowing vorticity bands is ruled out.

B. Gradient bands

We now argue that static *gradient* bands are also ruled out in steady state once particle migration is allowed for [see Fig. 6(b)]. We do not rule these out entirely, but analogous with the vorticity bands, we show that they should only arise under conditions where a system of fixed microscopic friction coefficient would also show gradient banding. This statement again relies on the fact that the state of friction, represented by f, can be viewed as a function of p_{yy} only. But separate equality of the fluid pressure and the normal-normal stress requires that p_{yy} and hence f is the same in coexisting gradient bands [35]. Accordingly, such bands can only exist if they would also do so in a system of fixed friction. As far as it is known, this does not happen for hard particles (but might do, very close to jamming, for deformable ones). A supplementary argument for the prohibition of gradient bands is provided in Appendix C.

C. Discussion

We have argued that neither vorticity nor gradient banding is generically sustainable in steady state for dense, shear-thickening suspensions of hard particles in which mechanical contact and viscous stresses remain unopposed by Brownian motion. Avoidance of mechanically induced particle migration then requires that the particle normal stress contributions p_{uu}, with u normal to the interface between bands, and the solvent pressure p_s, are separately equal in coexisting shear bands.

This condition holds only in strict steady state where all fluxes between bands must vanish. Quasi-steady shear bands could however be sustained under transient conditions by a nonzero flux of particles across the interface. One possible explanation of the data in [36], which apparently show static gradient bands, is that these represent a snapshot of the system while such fluxes remain transiently present [1,37]. (Note, however, that [36] used a wide-gap Couette system. In this, geometry banding is expected even for fixed-friction materials because the imposed ratio of shear to normal stress varies with radius, and may thus be unrelated to shear thickening.

The experimental fact, in any case, is that steady flow is not seen in our system whenever shear banding would be needed to create it. We have made similar observations on other materials than corn starch and we believe this to be the generic outcome for shear-thickening materials under conditions of imposed stress. We leave open the question of what to expect under conditions of imposed strain rate; since in fact only the average strain rate gets imposed, it is quite possible that an unsteady stress response will again arise close to the DST transition.

When steady banding is not possible, our experiments suggest that the dynamical outcome is as follows. The system jams locally (near the edge of our geometry, because the stress is largest at the edge of our parallel plates). The particles migrate away from the jammed region due to the unequal particle pressure in the jammed region. It is this local increase in particle pressure that drives particle migration that also deforms the meniscus. This migration continues until the pressures balance and locally the flow is no longer unstable and the system is unjammed. These jams always form at the edge of our sample, in a parallel plate geometry, due to the stress gradient over the sample. This explains how the system is able to flow deep into the regime where it would be expected to jam.

While we have ruled out stable bands in suspensions of non-Brownian hard particles, in Brownian suspensions, stable shear bands might be possible. For stable bands, the solvent pressure difference across the interface between the

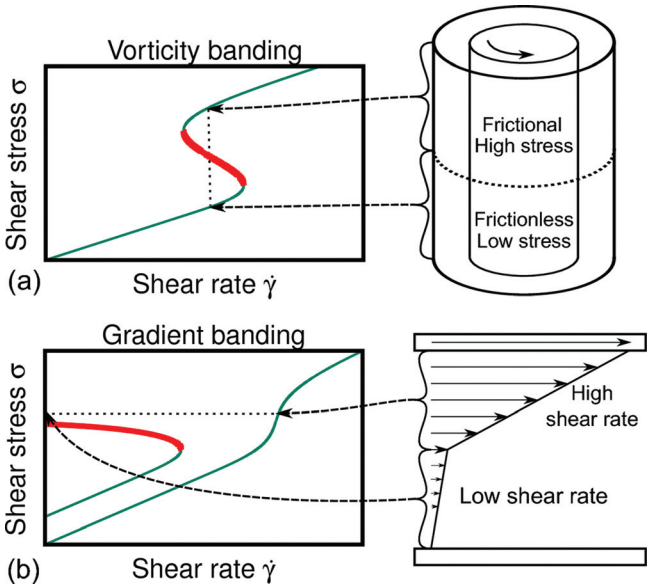

FIG. 6. (a) A schematic of vorticity banding as it could hypothetically occur for a homogeneous volume fraction. (b) A schematic of gradient banding as it could hypothetically occur in an inhomogeneous sample.

bands needs to be maintained. Without this, the particle pressures must be equal and the argument for non-Brownian systems forbids stable bands. In Brownian systems, such as micellar solutions and small hard-sphere colloids, osmotic forces can maintain an osmotic and thus a solvent pressure difference across an interface. For micelles, it is known that these unequal pressures cause differences in Laplace curvature at the external menisci of the two bands (which may fail if inequalities become large) [38]. In the non-Brownian suspensions studied here, the meniscus deforms (Fig. 3), indicating differences in pressure; however, these deformations are not stable. To stabilize the frictional shear band, the system needs to maintain a higher particle pressure (and thus a lower solvent pressure) in the frictional band than in the frictionless band. The mechanism required to stabilize the bands has to push particles from the frictionless band toward the frictional band and it has to do this against the particle pressure. Although Brownian motion is required, it might not be sufficient for the formation of stable bands. Equilibrium effects such as diffusion will never push hard colloidal particles against a pressure gradient. One way this can happen is through an out-of-equilibrium mechanism such as flow concentration coupling as in shear thickening micelles solutions [2,39]. Whether this is also possible for Brownian hard spheres remains to be investigated.

VI. CONCLUSION

The phenomenology of CST of non-Brownian suspensions is well described by the WC theory [9,15]. In this work, we have shown that the same applies in the DST regime, so long as one allows that the instability connected with a sigmoidal flow curve need not lead to the formation of steady-state vorticity bands. The steady banding picture would give two regimes with DST: one in which the bands comprise two different flowing states (the upper and lower quasi-Newtonian branches of the flow curve), at $\phi < \phi_m$; and one in which both the low-friction and the high-friction branch are not flowing, at $\phi > \phi_m$.

The latter is a strong prediction of any steady banding hypothesis since it implies that, above a relatively modest stress threshold $\sim 5\sigma^\star$, a static load can be supported indefinitely even though only part of the structure (the jammed bands) is contributing to its support. If true, this should presumably also be the case in other geometries of inhomogeneous stress, such as a person standing on a pool of corn starch suspension. If particle migration did not matter, the person should be able to stand still indefinitely without sinking in.

Contrary to the expectations based on any hypothesis of time-independent shear bands, we find that flow (although not steady) is possible even in this regime of very high density. The reason that the system is still capable of flow for $\phi > \phi_m$ is that it only spends part of its time in a jammed state. Whenever bands are present, particle migration allows the jammed regions to dilate and unjam. A new jam then forms somewhere else; bands are unsteady, and a finite average rate of flow is achieved. Even if the local stress exceeds the highest threshold calculated by WC, beyond which one expects homogeneous complete jamming rather than shear bands, particle migration into regions of lower stress will always allow motion to occur. This concurs with the observation that a pool of corn starch cannot in fact support a localized static weight for very long times [40]. According to our arguments, however, if this high threshold is exceeded across the entire sample, flow would finally cease. Hence, although one cannot stand still on an infinite pool of cornstarch suspension, it should be possible to do so on a finite bucket of the material.

If steady shear bands are indeed ruled out by our arguments, the ubiquitous unsteady flows that we observe stem naturally from the large, unstable, negative-slope region in the flow curves, predicted by the WC theory at ϕ values close to and beyond ϕ_m. We observed a transition from periodically jammed via intermittent to rheochaotic flows upon increasing the stress. Comparable behavior, while differing from system to system in the particular route to chaos (e.g., [41]), is well known for viscoelastic micellar solutions. It has even been observed for shear-thickening suspensions before, but was attributed then to wall slip [42]. This explanation is ruled out by the fact that we see the same phenomenology with and without hatched plates.

Combining the theoretical arguments leading to sigmoidal flow curves [15], with the case made above for the generic inadmissibility of shear-banded steady states, there is every reason to believe that our observations represent the inherent bulk rheology of very dense suspensions. Of course, the details of each unsteady flow, particularly in the chaotic regimes, may depend on the precise sample geometry. In particular, it may be influenced by the finite stress and/or strain-rate gradients imposed by all real rheometers. Nonetheless, it seems clear that unsteady flow is an intrinsic element of the rheology of very dense shear-thickening suspensions.

ACKNOWLEDGMENTS

The authors thank Suzanne Fielding, Peter Olmsted, and Romain Mari for discussions. This work was funded in part by EPSRC Grant No. EP/J007404. M.E.C. holds a Royal Society Research Professorship. B.G. was funded by a CASE scholarship with Johnson Matthey. Data relevant to this work have been archived and can be accessed at http://dx.doi.org/10.7488/ds/1393. M.W. thanks the Swiss National Science Foundation for support under Grant No. 200021-165509 and the Simons Collaborative Grant "Crackling the glass problem."

APPENDIX A: MACROSCOPIC FRICTION COEFFICIENTS

The detailed form of $\mu(\sigma_{xy},\phi)$ has not been reported for shear thickening systems although some work exists for viscous granular systems, which permanently occupy the high-σ shear-thickened state [9]. Imposed pressure measurements on frictional non-Brownian spheres [23] and 2D simulations of circular disks [24] found $\mu_{yy}(\phi)$ to be a monotonically decreasing function of ϕ, tending to a nonzero value μ_c at the jamming volume fraction ϕ_m, itself a function of the particle friction coefficient μ_p. Data for different μ_p including $\mu_p = 0$ collapse onto the same master curve in the 2D simulations. Since varying σ_{xy} essentially shifts the jamming volume fraction $\phi_J(\sigma_{xy})$ between ϕ_0 and ϕ_m, this collapse implies that $\mu = \mu(\phi)$ only. A σ_{xy}-dependence may exist in 3D, but we assume that this is small.

Deboeuf *et al.* [43] and Garland *et al.* [44] have measured the ϕ-dependence of the particle normal stress in the vorticity direction σ_{zz}, but did not report $\mu_{zz}(\phi)$ We can obtain μ_{zzz} indirectly via the second normal stress difference, N_2

$$\frac{N_2}{\sigma_{xy}} = \frac{1}{\mu_{yy}} - \frac{1}{\mu_{zz}}. \tag{A1}$$

For shear thickening dispersions, N_2 is typically small in magnitude and scales approximately with the shear stress for both continuous [45] and discontinuous [30] thickening, implying that the ratio μ_{zz}/μ_{yy} is independent of σ_{sy}. In granular suspensions, N_2/σ_{xy} has been found to vary only weakly with ϕ close to ϕ_m [46]. Together, these observations suggest that, in the range of ϕ we are considering, μ_{zz} is proportional to μ_{yy} and thus also slowly varying and monotonic.

When plotting Fig. 5(d), we took empirical expressions for $\mu_{yy}(\phi,\phi_m)$ from [23] up to ϕ_m using our value of $\phi_m = 0.56$ [solid line, Fig. 5(b), inset]; above ϕ_m we use the form in Fig. 5(c) (dashed line), which is a plausible extension of the curve given results from 2D simulations [24]. The curves for σ_{zz} (not shown) are qualitatively similar.

APPENDIX B: SUPPLEMENTARY ARGUMENT FOR PROHIBITION OF VORTICITY BANDS

Separate equality of p_s and p_{zz} between bands implies that for steady-state vorticity banding

$$\sigma_{xy}^{(1)}/\mu_{zz}^{(1)}(\phi_1, f(\sigma_{xy}^{(1)})) = \sigma_{xy}^{(2)}/\mu_{zz}^{(2)}(\phi_2, f(\sigma_{xy}^{(2)})). \tag{B1}$$

Suppose first that $\phi_1 = \phi_2$. The impossibility of Eq. (B1) being obeyed is then easily seen by thinking about the special case of σ-independent friction depicted in Fig. 5(d). With vorticity bands, a vertical line segment must be found connecting two different points on the same blue curve (common $\dot{\gamma}$ and ϕ but unequal shear stress). But this implies the existence of a similar line segment on the corresponding curve for p_{zz} (which closely resembles the red curve shown for p_{yy}) so that the relevant normal stress is also unequal.

A little thought shows the same to hold generically even when μ_{zz} depends on stress via $f(\sigma)$, so long as this dependence is reasonable, such as the expected smooth evolution between two order-unity limits as f varies from 0 to 1 [15]. Although exceptions might be created by fine-tuning the stress dependence of μ_{zz} in an exotic way, the generic physics is as follows. Steady vorticity bands are precluded because they need to be at the same particle pressure; but if they were, their frictional state and hence shear state would also be the same, leaving no difference between the bands.

Vorticity bands with unequal concentration, $\phi_1 \neq \phi_2$, can be excluded by a slight generalization of the same approach. Such bands require us to construct a vertical line connecting two blue curves such that the corresponding red curves are coincident at the chosen $\dot{\gamma}$. If μ is a slowly varying function of ϕ, then no two red curves ever coincide except at the origin [see Fig. 1(d)]. If $\mu_{zz}(\phi)$ is strongly decreasing close to ϕ_m, then one could construct a situation in which a high-σ_{xy}, low-0 phase coexists with a low-σ_{xy}, high-ϕ phase. [The converse situation arises when $\mu_{zz}(\phi)$ increases rapidly close to ϕ_m.] But in that case, the ratio of μ_{zz} at ϕ_1 and ϕ_1 and $\phi_2 < \phi_1$ must be comparable to the ratio of the viscosities of the limiting quasi-Newtonian regimes at ϕ_2

$$\frac{\mu_{zz}(\phi_2)}{\mu_{zz}(\phi_1)} \sim \frac{\eta(\sigma_{xy} \ll \sigma^\star, \phi_2)}{\eta(\sigma_{xy} \gg \sigma^\star, \phi_2)}. \tag{B2}$$

For the parameters used to generate the flow curves in Fig. 5, this requires $\mu_{zz}(\phi)$ to jump by a factor of $\mu_{zz}(0.553)/\mu_{zz}(0.558) \sim 10^2$ over a ϕ-range of 0.005. In the data of [23], Fig. 5(b), the change in $\mu_{yy}\phi$ is at most 10% over the same range. By this argument, even allowing for particle migration, steady-state vorticity bands are physically precluded by equality of p_{zz}.

APPENDIX C: SUPPLEMENTARY ARGUMENT FOR PROHIBITION OF GRADIENT BANDS

Gradient bands coexist at a common shear stress $\sigma_{xy}^{(1)} = \sigma_{xy}^{(2)}$ but different shear rates $\dot{\gamma}_1 \neq \dot{\gamma}_2$. The shear-thickening flow curves of interest have multivalued $\sigma(\dot{\gamma})$ but single-valued $\dot{\gamma}(\sigma)$. Crucially, this requires gradient bands always to have different concentrations, $\phi_1 \neq \phi_2$.

Mechanical stability now demands that the normal stress component in the velocity gradient direction is continuous across the band interface, $\sigma_{yy}^{(1)} = \sigma_{yy}^{(2)}$. Using the same arguments as before to rule out spatial variations in solvent pressure p_s, we find the condition

$$\mu_{yy}(\phi_1, f(\sigma_{xy}^{(1)})) = \mu_{yy}(\phi_2, f(\sigma_{xy}^{(2)})) = \mu_{yy}(\phi_2, f(\sigma_{xy}^{(1)})), \tag{C1}$$

where the last equality follows from the common shear stress in the two bands. Graphically, in reference to Fig. 5(d), steady gradient bands require us to find a horizontal

line that connects two flow curves at different ϕ (blue lines) such that the corresponding σ_{yy} values (red lines) are also equal. The latter is true if μ_{yy} is independent of ϕ (as was assumed for simplicity by WC), but is otherwise ruled out for monotonic but nonconstant $\mu_{yy}(\phi)$ of the kind generically expected in practice [compare Fig. 5(c)].

A possible exception again arises for the coexistence of a fully jammed state $(\phi > \phi_m, \dot{\gamma} = 0)$ with a flowing one $(\phi > \phi_m, \dot{\gamma} > 0)$. This outcome was reported in [36]; however, these authors used a wide-gap Couette system. In this geometry, "banding" is expected even for fixed-friction materials because the imposed ratio of shear to normal stress varies with radius. The interface between static and flowing "bands" is where this ratio crosses the static friction threshold set by the repose angle in the material.

Assuming a constant ratio $\sigma_{xy}/\sigma_{yy} = \mu_J$ within the jammed band, then our argument still holds so long $\mu_J - \lim \mu_{yy}(\phi \to \phi_m^-)$ is either zero (as expected by continuity arguments), or has the same sign as $d\mu_{yy}/d\phi$ (in effect, maintaining monotonicity). However, if μ_J is not constant but depends on other variables in the jammed state (such as a prior transient flow history or an elastic strain), gradient banding is not necessarily ruled out. Yet it would require the dense, frictional, jammed band to maintain as low a normal stress as a more dilute, less frictional, flowing one of equal σ_{xy}. As discussed above for the case of vorticity bands, this reverses the usual expectation concerning the relative dilatancy and/or friction of these two types of packing.

References

[1] Olmsted, P. D., "Perspectives on shear banding in complex fluids," Rheol. Acta **47**, 283–300 (2008).

[2] Cates, M. E., and S. M. Fielding, "Rheology of giant micelles," Adv. Phys. **55**, 799–879 (2006).

[3] Chakrabarti, B., M. Das, C. Dasgupta, S. Ramaswamy, and A. K. Sood, "Spatiotemporal rheochaos in nematic hydrodynamics," Phys. Rev. Lett. **92**, 055501 (2004).

[4] Einstein, A., "Über die von der molekularkinetischen theorie der warme geforderte bewegung von in ruhenden Flüssigkeiten suspendierten teilchen," Ann. Phys. **322**, 549–560 (1905).

[5] Batchelor, G. K., "The effect of Brownian motion on the bulk stress in a suspension of spherical particles," J. Fluid Mech. **83**, 97–117 (1977).

[6] Götze, W., *Complex Dynamics of Glass-Forming Liquids: A Mode-Coupling Theory* (Oxford University, Oxford, 2012).

[7] GadalaMaria, F., and A. Acrivos, "Shear-Induced structure in a concentrated suspension of solid spheres," J. Rheol. (1978-present) **24**, 799–814 (1980).

[8] Wilson, H. J., and R. H. Davis, "The viscosity of a dilute suspension of rough spheres," J. Fluid Mech. **421**, 339–367 (2000).

[9] Guy, B. M., M. Hermes, and W. C. K. Poon, "Towards a unified description of the rheology of hard-particle suspensions," Phys. Rev. Lett. **115**, 088304 (2015).

[10] Lin, N. Y. C., B. M. Guy, M. Hermes, C. Ness, J. Sun, W. C. K. Poon, and I. Cohen, "Hydrodynamic and contact contributions to continuous shear thickening in colloidal suspensions," Phys. Rev. Lett. **115**, 228304 (2015).

[11] Seto, R., R. Mari, J. F. Morris, and M. M. Denn, "Discontinuous shear thickening of frictional hard-sphere suspensions," Phys. Rev. Lett. **111**, 218301 (2013).

[12] Mari, R., R. Seto, J. F. Morris, and M. M. Denn, "Shear thickening, frictionless and frictional rheologies in non-Brownian suspensions," J. Rheol. **58**, 1693–1724 (2014).

[13] Mari, R., R. Seto, J. F. Morris, and M. M. Denn, "Nonmonotonic flow curves of shear thickening suspensions," Phys. Rev. E **91**, 052302 (2015).

[14] Ness, C., and J. Sun, "Shear thickening regimes of dense non-Brownian suspensions," Soft Matter **12**, 914–924 (2016).

[15] Wyart, M., and M. E. Cates, "Discontinuous shear thickening without inertia in dense non-Brownian suspensions," Phys. Rev. Lett. **112**, 098302 (2014).

[16] Melrose, J. R., and R. C. Ball, "The pathological behaviour of sheared hard spheres with hydrodynamic interactions," Europhys. Lett. **32**, 535–540 (1995).

[17] Melrose, J. R., J. H. van Vliet, and R. C. Ball, "Continuous shear thickening and colloid surfaces," Phys. Rev. Lett. **77**, 4660–4663 (1996).

[18] Morris, J. F., "A review of microstructure in concentrated suspensions and its implications for rheology and bulk flow," Rheol. Acta **48**, 909–923 (2009).

[19] Fernandez, N., R. Mani, D. Rinaldi, D. Kadau, M. Mosquet, H. Lombois-Burger, J. Cayer-Barrioz, H. J. Herrmann, N. D. Spencer, and L. Isa, "Microscopic mechanism for shear thickening of non-Brownian suspensions," Phys. Rev. Lett. **111**, 108301 (2013).

[20] Bender, J., "Reversible shear thickening in monodisperse and bidisperse colloidal dispersions," J. Rheol. **40**, 899–916 (1996).

[21] Note that the stress measured on the top plate is a combination of the first and second normal stress differences and not a measurement of the particles pressure as measured in [23].

[22] Grob, M., A. Zippelius, and C. Heussinger, "Rheo-chaos of frictional grains," Phys. Rev. E **93**, 030901 (2016).

[23] Boyer, F., É. Guazzelli, and O. Pouliquen, "Unifying suspension and granular rheology," Phys. Rev. Lett. **107**, 188301 (2011).

[24] Trulsson, M., B. Andreotti, and P. Claudin, "Transition from the viscous to inertial regime in dense suspensions," Phys. Rev. Lett. **109**, 118305 (2012).

[25] Lematre, A., J.-N. Roux, and F. Chevoir, "What do dry granular flows tell us about dense non-Brownian suspension rheology?," Rheol. Acta **48**, 925–942 (2009).

[26] Lerner, E., G. Düring, and M. Wyart, "A unified framework for non-Brownian suspension flows and soft amorphous solids," Proc. Natl. Acad. Sci. **109**, 4798–4803 (2012).

[27] Andreotti, B., J.-L. Barrat, and C. Heussinger, "Shear flow of non-Brownian suspensions close to jamming," Phys. Rev. Lett. **109**, 105901 (2012).

[28] DeGiuli, E., G. Düring, E. Lerner, and M. Wyart, "Unified theory of inertial granular flows and non-Brownian suspensions," Phys. Rev. E **91**, 062206 (2015).

[29] Bashkirtseva, I. A., A. Yu. Zubarev, L. Yu. Iskakova, and L. B. Ryashko, "On rheophysics of high-concentrated suspensions," Colloid J. **71**, 446–454 (2009).

[30] Laun, H. M., "Normal stresses in extremely shear thickening polymer dispersions," J. Non-Newtonian Fluid Mech. **54**, 87–108 (1994).

[31] Cates, M. E., M. D. Haw, and C. B. Holmes, "Dilatancy, jamming, and the physics of granulation," J. Phys.: Condens. Matter **17**, S2517–S2531 (2005).

[32] Pan, Z., H. de Cagny, B. Weber, and D. Bonn, "S-shaped flow curves of shear thickening suspensions: Direct observation of frictional rheology," Phys. Rev. E **92**, 032202 (2015).

[33] Fielding, S. M., and P. D. Olmsted, "Spatiotemporal oscillations and rheochaos in a simple model of shear banding," Phys. Rev. Lett. **92**, 084502 (2004).

[34] Andreotti, B., Y. Forterre, and O. Pouliquen, *Granular Media: Between Fluid and Solid* (Cambridge University Press, Cambridge, 2013).

[35] Recall that the normal-normal component of the particle stress is (minus) the diagonal component of the stress tensor. Thus if the z direction is the direction normal to the interface the normal-normal component is the z-z component of the stress tensor.

[36] Fall, A., F. Bertrand, D. Hautemayou, C. Mezire, P. Moucheront, A. Lematre, and G. Ovarlez, "Macroscopic discontinuous shear thickening versus local shear jamming in cornstarch," Phys. Rev. Lett. **114**, 098301 (2015).

[37] Adams, J. M., S. M. Fielding, and P. D. Olmsted, "Transient shear banding in entangled polymers: A study using the Rolie-Poly model," J. Rheol. (1978-present) **55**, 1007–1032 (2011).

[38] Skorski, S., and P. D. Olmsted, "Loss of solutions in shear banding fluids driven by second normal stress differences," J. Rheol. (1978-present) **55**, 1219–1246 (2011).

[39] Helfand, E., and G. H. Fredrickson, "Large fluctuations in polymer solutions under shear," Phys. Rev. Lett. **62**, 2468–2471 (1989).

[40] von Kann, S., J. H. Snoeijer, D. Lohse, and D. van der Meer, "Nonmonotonic settling of a sphere in a cornstarch suspension," Phys. Rev. E **84**, 060401 (2011).

[41] Ganapathy, R., and A. K. Sood, "Intermittency route to rheochaos in wormlike micelles with flow-concentration coupling," Phys. Rev. Lett. **96**, 108301 (2006).

[42] Larsen, R. J., J.-W. Kim, C. F. Zukoski, and D. A. Weitz, "Fluctuations in flow produced by competition between apparent, wall slip and dilatancy," Rheol. Acta. **53**, 333–347 (2014).

[43] Deboeuf, A., G. Gauthier, J. Martin, Y. Yurkovetsky, and J. F. Morris, "Particle pressure in a sheared suspension: A bridge from osmosis to granular dilatancy," Phys. Rev. Lett. **102**, 108301 (2009).

[44] Garland, S., G. Gauthier, J. Martin, and J. F. Morris, "Normal stress measurements in sheared non-Brownian suspensions," J. Rheol. **57**, 71–88 (2013).

[45] Cwalina, C. D., and N. J. Wagner, "Material properties of the shear-thickened state in concentrated near hard-sphere colloidal dispersions," J. Rheol. **58**, 949–967 (2014).

[46] Singh, A., and P. R. Nott, "Experimental measurements of the normal stresses in sheared Stokesian suspensions," J. Fluid Mech. **490**, 293–320 (2003).